PAPER

CrossMark
click for updates

Hyaluronic acid/poly-L-lysine bilayered silica nanoparticles enhance the osteogenic differentiation of human mesenchymal stem cells

Sara Amorim,[ab] Albino Martins,[ab] Nuno M. Neves,[ab] Rui L. Reis[ab] and Ricardo A. Pires*[ab]

Herein, we evaluate the influence of a PLL–HA bilayer on the surface of silica nanoparticles on their capacity to induce the osteogenic differentiation of human bone marrow stem cells (hBMSCs), as a function of their concentration (50 μg mL^{-1}, 25 μg mL^{-1} and 12.5 μg mL^{-1}). To this purpose, we synthesized silica nanoparticles (diameter of $\sim$250 nm; ζ-potential of -25 mV) that were coated with PLL–HA (diameter of $\sim$560 nm; ζ-potential of -35 mV). The cell viability, cell proliferation, protein quantification (i.e. MTS, DNA and ALP, respectively) and gene expression (of osteogenesis-related genes: ALP, osteocalcin, collagen type I, bone sialoprotein, Runx-2, osteopontin and osterix) were monitored, for 21 days. We observed the overexpression of most of the tested osteogenic transcripts in the hBMSCs cultured with SiO$_2$–PLL–HA, at concentrations of 25 μg mL^{-1} and 12.5 μg mL^{-1}. These results indicate that the proposed nanoparticles temporarily improve the osteogenic differentiation of hBMSCs at low nanoparticle concentrations.

1. Introduction

Bioceramics, bioactive glasses and related composite materials, that combine bioactive inorganic materials with biodegradable polymers,[1] have been extensively studied for biomedical applications.[2,3] Bioactive materials, in particular silica (SiO$_2$) nanoparticles, are considered relevant for bone tissue repair since: (i) they can be easily biofunctionalized; (ii) they are biocompatible (presenting osteoconductive and osteoinductive properties); and (iii) their degradation shows positive biological effects after implantation.[4,5] In addition, the size of SiO$_2$ nanoparticles can be tuned to match the size range of the integral parts of natural bone, such as hydroxyapatite crystals or cellular compartments, making them promising candidates for bone tissue regeneration.[6]

SiO$_2$ nanoparticles are usually obtained through the sol–gel methodology; they are produced by low-temperature processing, providing the conditions to synthesize nanoparticles of different compositions. In combination, these characteristics enable the preparation of monodispersive SiO$_2$ nanoparticles of different controllable sizes.[7]

Among the different techniques used to modify surfaces, the deposition of polyelectrolyte multilayers (PEMs) has emerged as a very easy handling and versatile tool. Based on the alternate adsorption of polycations and polyanions, this technique allows films to be built-up with tunable properties. Basically, this technique consists of the dipping of a material in a poly-electrolyte solution, which allows the interactions between a polycation and a polyanion, driving to the construction of a multilayered system.[8] Several studies have reported the construction of films onto charged surfaces (e.g. gold, SiO$_2$, etc.) using this layer-by-layer (LbL) technique exploiting the opposite charge of poly-L-lysine (PLL) and hyaluronic acid (HA).[9,10]

The HA is an important component of the natural extracellular matrix (ECM) being present in all tissues. It is a unique, linear, unmodified glycosaminoglycan consisting of repeating disaccharide units composed of D-glucuronic acid and D-N-acetylglucosamine. The HA functions not only as a structural component, but it can also bind to cells by direct interaction with cell surface receptors such as CD44. It is able to activate a series of intracellular signaling pathways, participating in the regulation of cell migration, proliferation and differentiation.[11,12] Some authors defend that HA induces an increase in the mesenchymal stem cell (MSC) differentiation onto the osteogenic lineage.[13] On the other hand, PLL, a cationic polymer at neutral pH, is commonly used as a cell-adhesion agent for cell-culturing experiments in plates and on other solid substrates.[14] The cationic primary amine groups of the lysine side chains interact with the negatively charged HA resulting in a multilayered system, well described in the literature.[15–17]

PLL–HA can be chemically cross-linked using water-soluble carbodiimide in combination with N-hydroxysulfosuccinimide. This cross-linked (PLL–HA)$_n$ system has been reported to

[a]3B's Research Group-Biomaterials, Biodegradables and Biomimetics, University of Minho, Headquarters of the European Institute of Excellence on Tissue Engineering and Regenerative Medicine, AvePark, 4806-909 Taipas, Guimarães, Portugal
[b]ICVS/3B's-PT Government Associate Laboratory, Braga/Guimarães, Portugal. E-mail: rpires@dep.uminho.pt

promote the anchoring of primary chondrocytes and smooth muscle cells, when compared to non cross-linked materials.[18] SiO$_2$ nanoparticles are known to be efficiently internalized into human MSCs without affecting cell viability, growth or differentiation.[19] MSCs represent a particularly interesting cell type for research and therapy because of their ability to differentiate into mesodermal lineage cells such as osteocytes, chondrocytes, cardiac muscle, and endothelial cells.[20] MSCs can been isolated from different organs and tissues, but the most relevant sources are the bone marrow and adipose tissue.

The present work describes the processing of bioactive organic/inorganic nanoparticles, exploiting their chemical and nano-topological structure, and their ability to induce human bone marrow MSC (hBMSC) differentiation towards the osteogenic lineage. Previous studies have reported that cells derived from bone marrow can be stimulated for osteogenesis when in contact with bioactive glasses.[21] Also, PEM systems, based on PLL–HA are reported to be capable of differentiating MSCs into osteocytes and chondrocytes upon culture with induction factors.[22] Taking advantage of the physico-chemical characteristics of SiO$_2$ nanoparticles and LbL construction, the overall aim of this work is to synthesize PLL–HA coated SiO$_2$ nanoparticles (Scheme 1) and to investigate their biological activity over viability, proliferation, and differentiation of hBMSCs.

2. Experimental

2.1 Materials

Tetraethyl orthosilicate 99% (TEOS), ammonium hydroxide solution (33%), poly-L-lysine (PLL; M_w 30–70 kDa), N-(3-dimethylaminopropyl)-N'-ethylcarbodiimide hydrochloride (EDC) $\geq$ 98.0% and N-hydroxysuccinimide (NHS) were obtained from Sigma-Aldrich. Hyaluronic acid (HA; M_w 1.20–1.80 MDa) was purchased from Lifecore. All the chemicals were used without further purification. For immunostaining we used phalloidin–tetramethylrhodamine B isothiocyanate (P1951) and 4,6-diamidino-2-phenylindole, dilactate (DAPI) (D9564) from Sigma-Aldrich. Primary antibodies osteocalcin (ab13418 – mousse anti-human) and osteopontin (ab14175 – rabbit anti-human) were purchased from AbCam. Secondary antibodies IgG Alexa Fluor® 488 (A-21202, anti-mouse) and IgG Alexa Fluor® 488 (A21206, anti-rabbit) were obtained from Invitrogen (Life Technologies).

2.2 Methods

Synthesis of silica nanoparticles. The synthesis of SiO$_2$ nanoparticles was performed as described elsewhere.[23] Briefly,
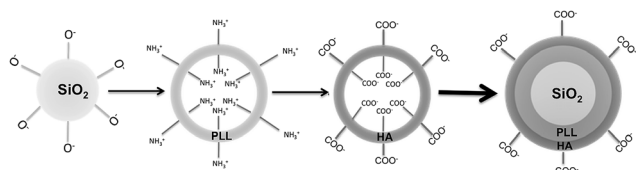
monodisperse spherical solid core SiO$_2$ nanoparticles were synthesized by mixing 8 mL of ammonium hydroxide with a solution containing 200 mL of absolute ethanol and 16 mL of deionized water. After stirring for 30 min, 24 mL of TEOS was added to the solution and stirred for 6 h at room temperature. The as-synthesized SiO$_2$ nanoparticle suspension was centrifuged and dried at 70 °C overnight. The resulting dry powder was further calcined at 550 °C for 6 h in air in order to remove organic residues.

Surface coatings. SiO$_2$ nanoparticles were immersed sequentially into a polycation and polyanion solutions, namely PLL (0.5 mg mL^{-1}) and HA (1 mg mL^{-1}), dissolved in 0.15 M NaCl (pH $\approx$ 5.5–6.0) to form the polymeric bilayer shell. Each layer was allowed to form for 15 minutes, followed by a set of three rinsing steps using a 0.15 M NaCl aqueous solution. After the formation of the bilayer, the polymeric shell was cross-linked using a mixture of water-soluble EDC (400 mM) and NHS (100 mM), as described elsewhere.[24] The nanoparticles were stirred overnight at 4 °C within the cross-linking solution (prepared with 0.15 M NaCl, pH $\approx$ 5.5–6.0). They were finally rinsed three times with a 0.15 M NaCl solution, generating the SiO$_2$–bilayer hybrid system (SiO$_2$–PLL–HA).

Surface morphology, size distribution and ζ-potential measurements. The surface morphology of the nanoparticles was examined using a scanning electron microscope (SEM; Leica S360, Cambridge, UK). The nanoparticles were coated with gold before the analysis. The size distribution of the nanoparticles, and their ζ-potential, were determined by Dynamic Light Scattering (DLS; Malvern, Zetasizer NANO-ZS).

Chemical analysis of the bilayered system. The surface chemistry of the nanoparticles was analyzed by Fourier transform infrared spectroscopy (FTIR). The samples were mixed with potassium bromide (KBr) in a ratio of 1 : 10, sample : KBr (w/w). The mixture was molded into a transparent pellet using a press (Pike, USA). Transmission spectra were acquired on an IR Prestige-21 spectrometer (Shimadzu, Japan), using 32 scans, a resolution of 4 cm^{-1} and a wavenumber range between 4400 cm^{-1} and 500 cm^{-1}.

Expansion, seeding and osteogenic differentiation of hBMSCs. hBMSCs were isolated from bone marrow aspirates of three donors, under established cooperative agreements between local Hospitals and the 3B's Research Group. The isolation procedure was performed according to the method established by Delorme and Charbord[25] and the characterization of the mesenchymal phenotype has been described in previous reports.[26–28] hBMSCs were expanded in basal medium consisting of Dulbecco's modified Eagle's medium (DMEM; Sigma-Aldrich, Germany) supplemented with 10% heat-inactivated fetal bovine serum (FBS; Biochrom AG, Germany) and 1% antibiotic/antimyotic solution (final concentration of penicillin 100 units mL^{-1} and streptomycin 100 mg mL^{-1}; Gibco, UK). Cells were cultured in a 5% CO$_2$ incubator at 37 °C.

Before the *in vitro* studies, the SiO$_2$–PLL–HA nanoparticles were sterilized by using ethylene oxide. Confluent hBMSCs, at passage 4, were harvested, seeded at a density of 1×10^5 cells per well of a 24 well-plate and cultured in the presence of the nanoparticles at concentrations of 50, 25 and 12.5 μg mL^{-1}, for

Scheme 1 LbL deposition of PLL and HA onto the surface of the SiO$_2$ nanoparticles.

7, 14 and 21 days under static conditions, in standard osteogenic differentiation medium (basal medium supplemented with 50 mg mL^{-1} ascorbic acid, 10^{-2} M β-glycerophosphate and 10^{-7} M dexamethasone). The assay control condition (SiO$_2$ nanoparticles without bilayer) at 50 μg mL^{-1} and positive control, were also cultured under standard osteogenic differentiation medium (basal medium supplemented with 50 μg mL^{-1} ascorbic acid, 10 mM β-glycerophosphate and 10^{-7} M dexamethasone).

Cell morphology and distribution. hBMSC samples were fixed with 2.5% glutaraldehyde (Sigma, Germany) in phosphate buffer saline solution (PBS; Sigma, Germany) and then dehydrated through an increasing series of ethanol concentrations (10%, 20%, 30%, 50%, 70%, 80%, 90% and 100%) and left to dry overnight. Finally, they were gold sputter-coated (Fisons Instruments SC502, UK) and observed by SEM (Leica S360, Cambridge, UK).

Cell viability and proliferation (MTS assay and DNA content). The hBMSC viability for each culturing time was determined using the Cell Titer 96® Aqueous One Solution Cell Proliferation Assay (Promega, USA). This assay is based on the bioreduction of a tetrazolium compound, 3-(4,5-dimethylthiazol-2-yl)-5-(3-carboxymethoxyphe-nyl)-2-(4-sulfofenyl)-2H-tetrazolium (MTS), into a water-soluble brown formazan product. NADPH or NADH production accomplishes this conversion by the dehydrogenase enzymes in metabolically active cells. The absorbance was measured at 490 nm using a microplate reader (Synergie HT, Bio-Tek, USA), being related to the quantity of formazan product.

Cell proliferation was quantified by the total amount of double-stranded DNA along the culturing time. Quantification was performed using the Quant-iT PicoGreen® dsDNA Assay Kit (Invitrogen, Molecular Probes, Oregon, USA), according to the manufacturer's instructions. Briefly, hBMSCs were lyzed by osmotic and thermal shock and the supernatant used for the DNA quantification assay. A fluorescent dye, PicoGreen, was used because of its high sensitivity and specificity to double-stranded DNA. The fluorescence of the dye was measured at an excitation wavelength of 485/20 nm and at an emission wavelength of 528/20 nm, in a microplate reader (Synergie HT, Bio-Tek, USA). Triplicates were carried out for each sample and per culturing time. The DNA concentration for each sample was calculated using a standard curve (DNA concentration ranging from 0.0 to 1.5 mg mL^{-1}) relating the quantity of DNA with the fluorescence intensity.

Alkaline phosphatase quantification. The concentration of alkaline phosphatase (ALP) was determined for all the culture time periods, using the same samples used for DNA quantification. Briefly, the activity of ALP was assessed using the *p*-nitrophenol assay. Nitrophenyl phosphate disodium salt (pnPP; Fluka BioChemika, Austria), which is colorless, is hydrolyzed by ALP at pH = 10.5 and a temperature of 37 °C to form free *p*-nitrophenol, which is yellow. The reaction was stopped by the addition of 2 M NaOH (Panreac Quimica, Spain) and the absorbance was read at 405 nm in a microplate reader (Synergie HT, Bio-Tek, USA). Standards were prepared with 10 μmol mL^{-1} of *p*-nitrophenol (pNP; Sigma, USA) solution, to obtain a standard curve ranging from 0.0 to 0.3 μmol mL^{-1}. Quadruplicates of each sample and standard were used, and the ALP concentrations were calculated from the standard curve.

RNA isolation and real-time quantitative Polymerase Chain Reaction (qPCR). The total RNA was extracted from the hBMSCs using the Tri® reagent (Sigma-Aldrich, USA), according to the manufacturer's instructions. Briefly, at each culturing time, the samples were washed with PBS, immersed in Tri reagent and stored at −80 °C, until further use. Proteins were removed with chloroform extraction, and the RNA pellets were washed once with isopropyl alcohol and once with 70% ethanol. Afterwards, the total RNA pellets were reconstituted in RNAse-free water (Gibco, Invitrogen, UK). Reverse transcriptase (RT)-PCR was performed according to the protocol from the iScript cDNA synthesis kit (Quanta BioSciences™, Gaithersburg, MD, USA). Briefly, a reaction mixture consisting of 1X iScript reaction mix, 1 mL iScript reverse transcriptase, RNA template (up to 1 mg total RNA) and nuclease-free water was prepared in 20 mL of total volume. The single-strand cDNA synthesis occurred by incubating the complete reaction mixture for 5 min at 25 °C, followed by 30 min at 42 °C, and was then terminated by an incubation at 85 °C for 5 min. Amplification of the target cDNA for real-time PCR quantification was performed according to the manufacturer's instructions, using 2 mL of RT cDNA products, 10^{-6} M of each primer 1XiQSYBR Green Supermix (Quanta BioSciences™, Gaithersburg, MD, USA) and nuclease-free water, in a final volume of 20 μL. 44 cycles of denaturation (95 °C, 10 s), annealing (temperature dependent on the gene, 30 s) and extension (72 °C, 30 s) were carried out in a Mastercycler Epgradient SRealplex Thermocycler (Eppendorf, Hamburg, Germany) for all genes. The transcripts' expression data were normalized to the housekeeping gene *glyceraldehyde-3-phosphate-dehygrogenase* (GAPDH) and the relative quantification calculated according to the Livak ($2^{-\Delta\Delta CT}$) method using the standard osteogenic culture condition as the calibrator.

Immunocytochemistry. Osteopontin (OP) and osteocalcin (OCN) protein expression of hBMSCs was assessed by immunofluorescence to evaluate the osteoblastic differentiation. hBMSCs grown in tissue culture coverslips were fixed in 10% formalin and stored at 4 °C in PBS. Samples were permeabilized with 0.025% of Triton X-100/PBS and washed twice with PBS. A 3% BSA/PBS solution was used to block unspecific binding of the antibodies, with an incubation of 45 min. Afterwards, samples were incubated in the diluted primary antibody solution (osteopontin (1 : 50) or osteocalcin (1 : 25)) in 1% BSA/PBS solution overnight at 4 °C. Samples were rinsed in permeabilization buffer and washed for 10 min in PBS, followed by incubation with the respective secondary fluorochrome-conjugated antibody for 2 h at room temperature in the dark. Finally, samples were incubated with DAPI solution (1/1000), for 15 min for nuclei staining, followed by incubation with phalloidin (1/100) for cytoskeletal labeling. Samples were washed with PBS before observation. An Olympus FluoView™ FV1000 confocal laser scanning microscope (CLSM) was used to acquire the images.

Statistical analysis. The normality of the data distribution was evaluated using the Shapiro–Wilk test ($p < 0.05$). Since the

data did not follow a normal distribution, an initial Kruskal–Wallis test was executed, followed by Dunn's post-test, with a significance level of 95% (for cell proliferation, viability and ALP activity). For the comparisons between groups, t-tests were performed (qPCR). In all cases, * indicates a significant difference with $p < 0.05$, ** with $p < 0.01$ and *** with $p < 0.001$.

3. Results and discussion

3.1 Particles characterization

SiO_2 nanoparticles were synthesized using a Stöber-like approach[29] in order to obtain a monodisperse particle size distribution.[30] The SiO_2 particle size distribution was determined by DLS (Table 1), confirming their monodispersive character, with an average diameter of 240 nm. The SEM microscopy (Fig. 1) is in agreement with this data, revealing that the nanoparticles present a spherical morphology, with an average diameter of $\sim$250 nm.

The functionalization of the surface of the SiO_2 nanoparticles with PLL and HA was executed using the LbL methodology.[31–33] PLL was used to coat the negatively charged Si–OH surface, followed by HA. The assembling of this bilayered system was followed by the ζ-potential of the SiO_2 nanoparticles before and after the coating with PLL and PLL–HA (Table 1).

The synthesized SiO_2 nanoparticles presented a ζ-potential of -25 mV at a pH $\sim$ 6, that, upon coating with PLL, changed to $+51$ mV due to the positive charge of its amine pending groups. The surface charge is again switched to negative (ζ-potential of -35 mV) with the coating of HA onto the PLL-coated SiO_2. These data are complemented with the SEM characterization, which confirms the maintenance of a spherical shape after the PLL–HA coating. The SEM image of the SiO_2–PLL–HA nanoparticles also revealed that their average diameter is $\sim$400 nm, while the DLS data indicate an average diameter of 567 nm. This mismatch can be explained by the hydration of the polymeric surface bilayer. While the SEM analysis is executed on dry samples and under vacuum, the DLS data are acquired while the nanoparticles are maintained on an aqueous suspension, which enables the hydration of the polymeric coating. In fact, HA is known for its high hydration capacity that increases its dimensions in solution.[34]

The FTIR spectra of PLL, HA, SiO_2 and SiO_2–PLL–HA are presented in Fig. 2, while the PLL and HA typical IR peaks (with their corresponding assignments) are listed in Table 2.[9,35,36] The ν(NH) at 3285 cm^{-1} is clearly visible in the PLL spectrum, and its contribution to the SiO_2–PLL–HA spectrum is observed as a
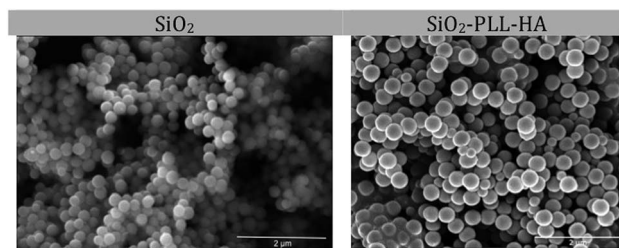

Fig. 1 SEM micrographs of the synthesized SiO_2 and SiO_2–HA–PLL nanoparticles.

large shoulder to lower wavenumbers of the peak at 3400 cm^{-1} (ν(OH) from HA and SiO_2). The peaks from the ν_{as}(COO$^-$) of HA at 1655 cm^{-1} and from the ν(C=O) of PLL at 1658 cm^{-1} are observed in the spectrum of SiO_2–PLL–HA at 1660 cm^{-1}.[36] The HA spectrum also reveals its ν_s(COO$^-$) at 1411 cm^{-1}, whose contribution to the SiO_2–PLL–HA spectrum is in the form of a small shoulder at higher wavenumbers, 1520 cm^{-1}. The asymmetric vibration of the ν(SiO) with a strong absorption peak at 1090 cm^{-1} also reveals an enlargement due to the influence of HA characteristic peaks.[37] Finally, the presence of HA in the SiO_2–PLL–HA is further confirmed by the observation in its spectrum of the δ(COO$^-$) of HA at 900 cm^{-1}.

The collected data confirm the synthesis of monodisperse core–shell nanoparticles (SiO_2–PLL–HA) with SiO_2 acting as a core and the LbL assembled bilayer of PLL–HA as a shell.

3.2 Improvement of the hBMSCs' osteogenic differentiation in the presence of the nanoparticles

Cell morphology, proliferation and viability. The effect of SiO_2 concentration on cell viability and proliferation, and particularly on the osteogenic differentiation is widely reported in the literature. Huang et al.[5] showed that mesoporous SiO_2 nanoparticles, at concentrations ranging from 4 to 200 μg mL^{-1}, do not affect the viability and proliferation of hMSCs. This study concluded that hMSCs exposed to 40 μg mL^{-1} of nanoparticles for three days expressed a significant but transient osteogenic signal of ALP. On the other hand, Kim et al.[38] reported that mRNA expression levels of OCN and OP, evaluated on human adipose-derived stem cells cultured in standard osteogenic differentiation medium, were higher in the medium containing 98.7 μg mL^{-1} of silicate ions, when compared to 470 μg mL^{-1} of silicate ions in the culture medium. Finally, Shen et al.[39]

Table 1 Size and ζ-potential of the SiO_2, SiO_2–PLL and SiO_2–PLL–HA nanoparticles

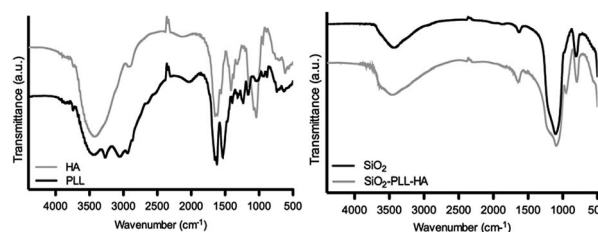| Materials	Diameter^a (nm)	PDI	ζ-Potential (mV)
SiO_2	240.2 ± 10.9	0.124 ± 0.01	-25.0 ± 0.7
SiO_2–PLL	270.3 ± 6.7	0.150 ± 0.01	50.6 ± 4.1
SiO_2–PLL–HA	567.6 ± 6.5	0.120 ± 0.03	-34.9 ± 5.2

^{a} Determined by DLS.

Fig. 2 FTIR spectra of the PLL, HA, SiO_2 and SiO_2–PLL–HA after crosslinking with EDC–NHS.

Table 2 Typical vibrational modes of the PLL and HA chemical groups and their wavenumber assignments

Chemical bond	Wavenumber (cm^{-1})
$\nu(OH)$ hydroxyl groups of HA	3400
$\nu(NH)$ amine groups of PLL	3285
$\nu(NH)$ amine groups of PLL	1658
$\nu_{as}(COO^-)$ carboxylate anion of HA	1655
$\nu_s(COO^-)$ carboxylate anion of HA	1411
$\nu(COO^-)$ carboxylate anion of HA	900

demonstrated that 50 µg mL^{-1} of SiO_2-based nanoparticles cultured with MSCs successfully differentiated into osteocytes, as demonstrated by ALP activity. Furthermore, this SiO_2 concentration did not significantly affect cell viability and proliferation. Based on these results, 50 µg mL^{-1} was set as the maximum concentration of nanoparticles in the culture medium for the present study.

The synthesized nanoparticles were seeded directly onto cultured hBMSCs, for different time periods (7, 14 and 21 days) and investigated in terms of their genotypic and phenotypic features. The morphology of hBMSCs in contact with SiO_2 and SiO_2–PLL–HA (50, 25 and 12.5 µg mL^{-1}, named SiO_2–PLL–HA, SiO_2–PLL–HA(1/2) and SiO_2–PLL–HA(1/4), respectively) was analysed by SEM (Fig. 3). The hBMSCs exhibited the typical spindle-shape morphology and cell-to-cell interactions were also observed as previously reported.[40]

The effect of SiO_2–PLL–HA nanoparticles, at different concentrations, on hBMSC proliferation was also assessed by measuring the total cells' DNA (Fig. 4). Previous studies of hBMSC response to SiO_2 nanoparticles revealed no evidence of cytotoxicity for 1–3 days of incubation.[5,39,41] From our data, the same behaviour is observed at days 7, 14 and 21 for the silica and bilayered silica nanoparticles at all studied concentrations. Furthermore, hBMSC proliferation results do not show statistically significant differences between the cells cultured with and without nanoparticles at the same time points.

A metabolic activity-based assay (MTS) was also performed at the different time points, in order to determine the hBMSC viability when cultured in osteogenic culture medium. MTS results are directly proportional to the number of living cells.[42] Our results (Fig. 4) indicate that, at day 7, SiO_2 nanoparticles at a concentration of 50 µg mL^{-1} show a higher viability when compared to the osteogenic control, indicating that those nanoparticles are not cytotoxic. At the same time point, the hBMSCs cultured with SiO_2–PLL–HA(1/2) and SiO_2–PLL–HA(1/4) nanoparticles present a highly significant increase on viability, when compared to the control. These conditions have a different behaviour than the SiO_2–PLL–HA. In the latter case, the cells present a viability comparable to the control. Therefore, a lower concentration of bilayered silica nanoparticles induces a higher hBMSC metabolic activity. At day 21, no significant differences were observed, except for SiO_2–PLL–HA which presents a significantly lower ($p < 0.05$) metabolic activity than the cells cultured with SiO_2–PLL–HA(1/2).

Genotypic characterization of differentiated hBMSCs. Complementary to the reported biological data, the differentiation level of hBMSCs cultured with SiO_2 and SiO_2–PLL–HA nanoparticles was assessed by quantitative PCR of some bone-specific gene transcripts, namely, ALP, OP, OCN, bone sialoprotein (BSP), osterix (OSX), Runx-related transcription factor 2 (Runx-2) and collagen type I (Colα). The relative expression of those genes was normalized against the housekeeping gene GAPDH and the standard osteogenic culture condition was used as the calibrator. It is well described that the osteogenic differentiation can be subdivided into several developmental stages: proliferation of stem cells, ECM synthesis, maturation and ECM mineralization, each with characteristic changes in the gene expressions rates.[43]

In this study, each selected gene is responsible for different stages of differentiation. The transcription factor Runx-2 is a crucial early marker of the MSCs commitment at the osteogenic lineage. Runx-2 up-regulates BSP and OCN, two major components of the bone ECM synthesized exclusively by osteoblastic cells.[44] While BSP is an osteoblast-enriched gene,[45] OCN is the major non-collagenous protein component of bone ECM and secreted exclusively by osteoblastic cells at the late stage of
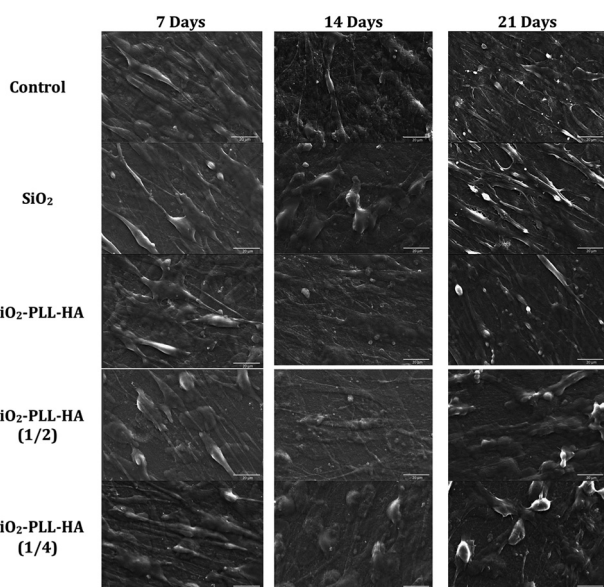
Fig. 3 SEM micrographs of the morphology of hBMSCs cultured for 7, 14 and 21 days with SiO_2 and SiO_2–PLL–HA nanoparticles.
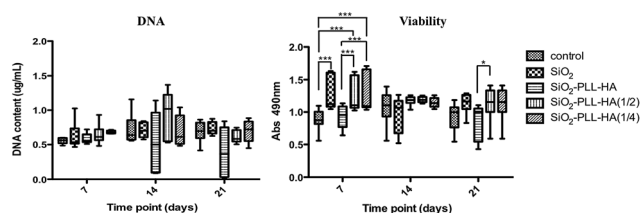
Fig. 4 hBMSC proliferation (DNA quantification) and viability (MTS quantification) at 7, 14, and 21 days after seeding. Significant differences were represented by * for $p < 0.05$, ** for $p < 0.01$ and *** for $p < 0.001$, as determined by the statistical analysis.

maturation, and therefore is considered as an indicator of osteoblast differentiation.[46]

From the PCR data (Fig. 5) it is clear that there is an up-regulation of Runx-2 in the cells cultured with SiO_2–PLL–HA(1/4) at 14 days and SiO_2–PLL–HA(1/2) at 7 days. In fact, the OCN and BSP (usually linked to the Runx-2 expression) are also overexpressed at the same time point and bilayered nanoparticles' concentration. Unexpectedly, at higher nanoparticle concentrations, SiO_2–PLL–HA, we did not observe the same trend in the Runx-2 expression. These observations might be related to the overexpression of Runx-2 in between the time points chosen for this study, which would limit its detection by PCR. In the SiO_2 case, Runx-2 is overexpressed at 7 days of culture, although the up-regulation of OCN and BSP is not observed for SiO_2 at any time point. Our data indicate that the SiO_2–PLL–HA(1/2) and SiO_2–PLL–HA(1/4) present the most consistent enhancement of the hBMSC osteogenic differentiation, through the early osteogenic marker Runx-2, which also promotes the overexpression of the BSP and OCN genes.

OSX is one of the few characterized osteoblast specific genes.[47] It is known to be a specific osteogenic transcription factor, which is identified as a late bone marker required for the differentiation of preosteoblasts into fully functioning osteoblasts.[48] The OSX gene expression results showed that, at day 14, SiO_2–PLL–HA(1/4) presents the highest OSX overexpression, which indicates higher osteogenic activity. These results are consistent with the observed overexpression of the OCN and BSP under the same culture conditions (i.e. 14 days and SiO_2–PLL–HA(1/4)).

OP performs important bone related functions, although, it cannot be considered bone specific since it also plays roles in kidneys, epithelial lining tissues, blood plasma, and breast milk.[47] Despite this, its gene expression evaluation was not discarded. OP appears up-regulated mostly at days 7 and 14 for the SiO_2–PLL–HA(1/2) condition. The Colα, as OP, cannot be considered bone specific, having been identified in numerous unrelated cell types. However, it is expressed at high levels near to the end of the proliferative period, which occurs until day 7 of culture, and during the period of ECM deposition and maturation.[49] In fact, Colα gene expression is up-regulated mainly at day 14 in the presence of SiO_2–PLL–HA(1/4) and at day 7 for the SiO_2–PLL–HA(1/2). This observation is in accordance with its typical early stage expression.

Finally, another bone non-specific gene is the ALP, which is also expressed at the early stages of the osteogenic differentiation. At day 7 and 14 we registered an increase of ALP expression in the cells cultured in the presence of SiO_2–PLL–HA(1/2) and SiO_2–PLL–HA(1/4), respectively. These observations are consistent with the overexpression of the other monitored genes for the same samples, which also showed an up-regulation of genes Runx-2, OSX, OCN, BSP and Colα, at the same time points. Summarizing, the gene expression shows relevant differences in coated silica nanoparticles with PLL–HA, at lower concentrations, than the SiO_2 nanoparticles. In fact, Manferdini et al.[50] described that the biomimetic treatment of an HA-based scaffold promotes a faster mineralization process, suggesting its possible use in clinics as a support for improving bone repair.

ALP activity quantification. ALP, an early stage marker of osteogenic differentiation, is an enzyme belonging to a group of membrane-bound glycoproteins, involved in the pathway resulting in the deposition of minerals on ECM molecules.[51] The ALP activity of hBMSCs was assessed as an indicator of the osteogenic differentiation. Fig. 6 presents the ALP protein activity expression profiles (μmol ALP per mg protein) of cultured hBMSCs. The results show that ALP activity values increase progressively with time under all the different experimental conditions, except for the SiO_2–PLL–HA that presents a peak at day 14 and a decrease in the following time point (this is also in accordance with the gene expression analysis, where the ALP gene expression is down-regulated mainly at the latter time points).

In general, the cells' ALP genetic expression is usually observed before the ALP is actually synthesized by the cells. In this context, and analyzing these data in combination with the ALP genetic expression profiles, an increase on the activity of the protein at higher time points would be expected, as observed for the cells cultured in the presence of lower concentration of bilayered nanoparticles, i.e. SiO_2–PLL–HA(1/2) and SiO_2–PLL–HA(1/4).
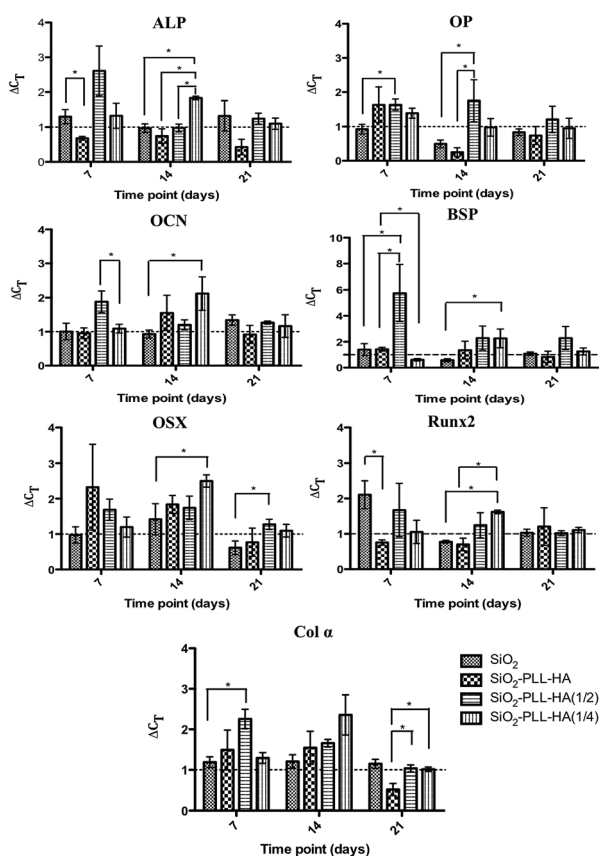

Fig. 5 Relative expression of bone-specific transcripts, namely ALP, OP, BSP, OCN, Runx-2, OSX and Colα by hBMSCs induced the differentiation into the osteogenic lineage over 21 days. The results are expressed as the means ± SD, (*) indicating a significant difference with $p < 0.05$, (**) $p < 0.01$, and (***) $p < 0.001$. The dashed line indicates the normalized gene expression of the standard osteogenic culture conditions.
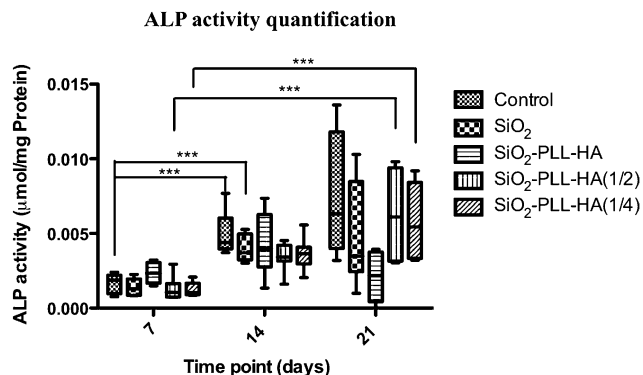
ALP activity quantification

Fig. 6 ALP activity of hBMSCs cultured with SiO_2 and $SiO_2-PLL-HA$ nanoparticles at time points 7, 14 and 21 days, under osteogenic induction.

Phenotypic characterization of differentiated hBMSCs. The immunofluorescence staining of matrix-associated proteins (OCN and OP) were used as markers of hBMSCs osteoblastic differentiation. OCN, a bone-specific glycoprotein that binds calcium and may promote calcification of the bone ECM, has been used as a late marker of the osteogenic differentiation.[52] OP, synthesized by bone forming cells, is also a phosphoprotein that possesses several calcium-binding domains and is associated with cell attachment, proliferation, and mineralization of the bone ECM.[52] Fig. 7 shows the fluorescence of the OP and OCN markers.

In the case of OP, as expected, a delay in the protein synthesis and its genetic expression is observed. In fact, in all the cases, there is an initial higher genetic expression (PCR data) that is accompanied by the protein synthesis at a latter stage. As an example we observe an OP genetic overexpression

(compared to the control group) in days 7 and 14 for the $SiO_2-PLL-HA(1/2)$ that is followed by a higher OP fluorescence in the cell culture at day 21.

In the case of OCN expression, its deposition in the ECM under all cultured conditions is clearly visible. Again the genetic up-regulation occurs at earlier time points (day 7 or 14) for the $SiO_2-PLL-HA$, $SiO_2-PLL-HA(1/2)$ and $SiO_2-PLL-HA(1/4)$ nanoparticles, although, the increase in the OP fluorescence is only observed at day 21 (compared to the control sample). This is again in accordance with the different timeframes of genetic expression and protein deposition, as previously explained.

4. Conclusions

Herein was demonstrated that the proposed SiO_2 bilayered system is able to improve the *in vitro* osteogenic differentiation of hBMSCs, which is dependent on the nanoparticle concentration, without detrimental effect over cell viability and proliferation. An early in time overexpression of ALP, OCN, OP, BSP, OSX, Runx-2 and Colα was observed when bilayered nanoparticles were used in the culture medium. The highest overexpression of these osteogenesis-related genes was observed at lower concentrations of nanoparticles (25 μg mL^{-1} and 12.5 μg mL^{-1}), being an indication of their osteoinduction activity. The study shows that bi-layered silica nanoparticles at low concentrations are potential candidates for applications in regenerative medicine. These systems can be used as injectable or a useful component of scaffolds for bone tissue regeneration approaches.

Acknowledgements

References

1 L.-C. Gerhardt and A. R. Boccaccini, *Materials*, 2010, **3**, 3867–3910.

2 R. Jugdaohsingh, *J. Nutr., Health Aging*, 2009, **11**, 99–110.

3 B. Lei, X. Chen, X. Han and J. Zhou, *J. Mater. Chem.*, 2012, **22**, 16906–16913.

4 B. Lei, X. Chen, X. Han and Z. Li, *J. Mater. Chem.*, 2011, **21**, 12725–12734.

5 D. Huang, T. Chung, Y. Hung, F. Lu, S.-H. Wu, C.-Y. Mou, M. Yao and Y.-C. Chen, *Toxicol. Appl. Pharmacol.*, 2008, **231**, 208–215.

6 A. Tautzenberger, A. Kovtun and A. Ignatius, *Int. J. Nanomed.*, 2012, **7**, 4545–4557.

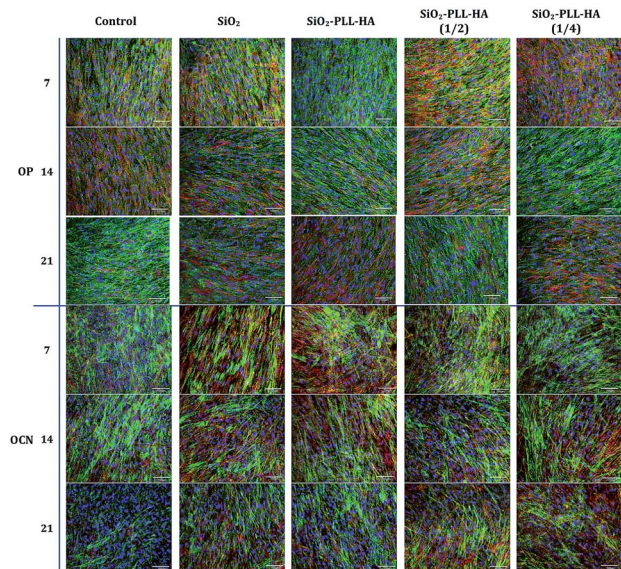7 J. Y. Wen and G. L. Wilkes, *Chem. Mater.*, 1996, **8**, 1667–1681.

Fig. 7 Confocal micrographs of the hBMSCs cultured in the presence of nanoparticles for 21 days. Nuclei were stained in blue, actin in red and OP or OCN in green.

8 L. Richert, F. Boulmedais, P. Lavalle, J. Mutterer, E. Ferreux, G. Decher, P. Schaaf, J.-C. Voegel and C. Picart, *Biomacromolecules*, 2004, **5**, 284–294.

9 L. Shen, P. Chaudouet, J. Ji and C. Picart, *Biomacromolecules*, 2011, **12**, 1322–1331.

10 C. Picart, P. Lavalle, P. Hubert, F. J. G. Cuisinier, G. Decher, P. Schaaf and J. C. Voegel, *Langmuir*, 2001, **17**, 7414–7424.

11 L. Zou, X. Zou, L. Chen, H. Li, T. Mygind, M. Kassem and C. Bünger, *J. Orthop. Res.*, 2008, **26**, 713–720.

12 J. Patterson, R. Siew, S. W. Herring, A. S. Lin, R. Guldberg and P. S. Stayton, *Biomaterials*, 2010, **31**, 6772–6781.

13 T. Sasaki and C. Watanabe, *Bone*, 1995, **16**, 9–15.

14 V. Krikorian, M. Kurian, M. E. Galvin, A. P. Nowak, T. J. Deming and D. J. Pochan, *J. Polym. Sci., Part B: Polym. Phys.*, 2002, **40**, 2579–2586.

15 L. Jourdainne, S. Lecuyer, Y. Arntz, C. Picart, P. Schaaf, B. Senger, J.-C. C. Voegel, P. Lavalle and T. Charitat, *Langmuir*, 2008, **24**, 7842–7847.

16 L. Richert, A. Schneider, D. Vautier, C. Vodouhe, N. Jessel, E. Payan, P. Schaaf, J. C. Voegel and C. Picart, *Cell Biochem. Biophys.*, 2006, **44**, 273–285.

17 T. Boudou, T. Crouzier, R. Auzely-Velty, K. Glinel and C. Picart, *Langmuir*, 2009, **25**, 13809–13819.

18 A. Engler, L. Richert, J. Wong, C. Picart and D. Discher, *Surf. Sci.*, 2004, **570**, 142–154.

19 A. K. Gaharwar, S. M. Mihaila, A. Swami, A. Patel, S. Sant, R. L. Reis, A. P. Marques, M. E. Gomes and A. Khademhosseini, *Adv. Mater.*, 2013, **25**, 3329–3336.

20 G. Brooke, M. Cook, C. Blair, R. Han, C. Heazlewood, B. Jones, M. Kambouris, K. Kollar, S. McTaggart, R. Pelekanos, A. Rice, T. Rossetti and K. Atkinson, *Semin. Cell Dev. Biol.*, 2007, **18**, 846–858.

21 M. Amaral, M. A. Costa, M. A. Lopes, R. F. Silva, J. D. Santos and M. H. Fernandes, *Biomaterials*, 2002, **23**, 4897–4906.

22 O. V. Semenov, A. Malek, A. G. Bittermann, J. Voros and A. H. Zisch, *Tissue Eng., Part A*, 2009, **15**, 2977–2990.

23 S. B. Yoon, J.-Y. J. H. Kim, Y. J. Park, K. R. Yoon, S.-K. Park and J.-S. Yu, *J. Mater. Chem.*, 2007, **17**, 1758.

24 K. Ren, L. Fourel, C. G. Rouviere, C. Albiges-Rizo and C. Picart, *Acta Biomater.*, 2010, **6**, 4238–4248.

25 B. Delorme and P. Charbord, *Methods Mol. Med.*, 2007, **140**, 67–81.

26 M. L. Alves da Silva, A. Martins, A. R. Costa-Pinto, V. M. Correlo, P. Sol, M. Bhattacharya, S. Faria, R. L. Reis and N. M. Neves, *J. Tissue Eng. Regener. Med.*, 2011, **5**, 722–732.

27 N. Monteiro, A. Martins, D. Ribeiro, S. Faria, N. A. Fonseca, J. N. Moreira, R. L. Reis and N. M. Neves, *J. Tissue Eng. Regener. Med.*, 2013, DOI: 10.1002/term.1817.

28 A. R. Costa-Pinto, V. M. Correlo, P. C. Sol, M. Bhattacharya, P. Charbord, B. Delorme, R. L. Reis and N. M. Neves, *Biomacromolecules*, 2009, **10**, 2067–2073.

29 I. Ibrahim, A. Zikry and M. Sharaf, *The Journal of American Science*, 2010, **6**, 985–989.

30 J. Chruściel and L. Ślusarski, *Mater. Sci.*, 2003, **21**, 461–469.

31 R. V. Klitzing, *Phys. Chem. Chem. Phys.*, 2006, **8**, 5012–5033.

32 A. P. R. R. Johnston, C. Cortez, A. S. Angelatos and F. Caruso, *Curr. Opin. Colloid Interface Sci.*, 2006, **11**, 203–209.

33 J. Jaber and J. Schlenoff, *Curr. Opin. Colloid Interface Sci.*, 2006, **11**, 324–329.

34 R. Novoa-Carballal, D. V. Pergushov and A. H. E. Müller, *Soft Matter*, 2013, **9**, 4297.

35 K. Haxaire, Y. Maréchal, M. Milas and M. Rinaudo, *Biopolymers*, 2003, **72**, 10–20.

36 M. Rozenberg and G. Shoham, *Biophys. Chem.*, 2007, **125**, 166–171.

37 A. Beganskienė and V. Sirutkaitis, *Mater Sci.*, 2004, **10**, 287–290.

38 K. Kim, J. Lee, S. Lee and J. Rhie, *J. Tissue Eng. Regener. Med.*, 2010, **7**, 171–177.

39 Y. Shen, Y. Shao, H. He and Y. Tan, *Int. J. Nanomed.*, 2013, **8**, 119–127.

40 P. Han, C. Wu and Y. Xiao, *Biomater. Sci.*, 2013, **1**, 379–392.

41 S. Labbaf, O. Tsigkou, K. H. Müller, M. M. Stevens, A. E. Porter and J. R. Jones, *Biomaterials*, 2011, **32**, 1010–1018.

42 A. Zonari, S. Novikoff, N. R. P. Electo, N. M. Breyner, D. A. Gomes, A. Martins, N. M. Neves, R. L. Reis and A. M. Goes, *PLoS One*, 2012, **7**, e35422.

43 D.-M. Huang, Y. Hung, B.-S. Ko, S.-C. Hsu, W.-H. Chen, C.-L. Chien, C.-P. Tsai, C.-T. Kuo, J.-C. Kang, C.-S. Yang, C.-Y. Mou and Y.-C. Chen, *FASEB J.*, 2005, **19**, 2014–2016.

44 A. Polini, D. Pisignano, M. Parodi, R. Quarto and S. Scaglione, *PLoS One*, 2011, **6**, e26211.

45 M-T. Tsai, Y-S. Lin, W-C. Chen, C-H. Ho, H-L. Huang and J-T. HSu, *Proceedings of the World Congress on Engineering*, 2011, **3**, 2690–2694.

46 G. Kirkham, S. Cartmell and N. Ashammakhi, in *Topics in Tissue Engineering*, ed. N. Ashammakhi, R. Reis and E.Chiellini, 2007, vol. 3.

47 E. Kärner, C. Bäckesjö and J. Cedervall, *Biochim. Biophys. Acta, Gen. Subj.*, 2009, **1790**, 110–118.

48 N. Chevallier, F. Anagnostou, S. Zilber, G. Bodivit, S. Maurin, A. Barrault, P. Bierling, P. Hernigou, P. Layrolle and H. Rouard, *Biomaterials*, 2010, **31**, 270–278.

49 M. Sila-Asna, A. Bunyaratvej, S. Maeda, H. Kitaguchi and N. Bunyaratavej, *Kobe J. Med. Sci.*, 2007, **53**, 25–35.

50 C. Manferdini, V. Guarino, N. Zini, M. G. Raucci, A. Ferrari, F. Grassi, E. Gabusi, S. Squarzoni, A. Facchini, L. Ambrosio and G. Lisignoli, *Biomaterials*, 2010, **31**, 3986–3996.

51 J. L. Whyte, S. G. Ball, C. A. Shuttleworth, K. Brennan and C. M. Kielty, *Stem Cell Res.*, 2011, **6**, 238–250.

52 G. Karsenty, *Genes Dev.*, 1999, **13**, 3037–3051.